Active Volcanoes of the World

Nick Varley · Charles B. Connor
Jean-Christophe Komorowski
Editors

Volcán de Colima

Portrait of a Persistently Hazardous Volcano

Springer

Active Volcanoes of the World

More information about this series at http://www.springer.com/series/10081

Nick Varley · Charles B. Connor
Jean-Christophe Komorowski
Editors

Volcán de Colima

Portrait of a Persistently Hazardous Volcano

Springer

Editors
Nick Varley
Facultad de Ciencias
Universidad de Colima
Colima, Mexico

Jean-Christophe Komorowski
Institut de Physique du Globe de Paris
Paris, France

Charles B. Connor
School of Geosciences
University of South Florida
Tampa, FL, USA

ISSN 2195-3589 ISSN 2195-7029 (electronic)
Active Volcanoes of the World
ISBN 978-3-642-25910-4 ISBN 978-3-642-25911-1 (eBook)
https://doi.org/10.1007/978-3-642-25911-1

Library of Congress Control Number: 2018959259

This Springer imprint is published by the registered company Springer-Verlag GmbH, DE part of Springer Nature
The registered company address is: Heidelberger Platz 3, 14197 Berlin, Germany

Preface

This volume summarizes some of the recent scientific works to characterize the eruptive history, magmatic system and hazards associated with Volcán de Colima (Mexico), one of the most continuously active composite volcanoes on Earth during the historic era. Indeed, the history of scientific investigation of Volcán de Colima parallels the history of volcano science as a whole. This is not surprising, because from the very beginning of volcano science, Volcán de Colima was recognized as a laboratory for observing and understanding fantastic and rare eruptive phenomena. The volcano has been the subject of an impressive range of studies, which together, have increased our knowledge of this beautiful stratovolcano, and thus provided a better chance of an effective risk reduction strategy for the future. Many of the observations and fresh theories that have been derived can easily be applied to similar systems worldwide. Each chapter in this volume builds upon this record of research, conducted by generations of scientists who have studied the volcano. It provides an overview of the state of our knowledge, and will serve as a launching point for new initiatives in the forthcoming years.

Medina (1983) reports that the earliest records of Volcán de Colima eruptions were compiled in the 'Archivo de Indias', a library commissioned in 1572 by Philip II in Seville (Spain). These records include reports on eruptions in 1560 and large, possibly Plinian, eruptions in 1576 C.E. and 1585 C.E. The record of eruptive activity throughout the sixteenth–early nineteenth centuries was compiled from scattered reports by Arreloa (1903, 1915), Bárcena (1887) and Ordonez (1897), and was later summarized concisely by Mooser (1958, 1961). Charles Lyell mentions the 1818 C.E. eruption of Volcán de Colima in his famous text, Principles of Geology (Lyell 1830), but erroneously attributes the eruption to the reactivation of Volcán Jorullo. He writes that 6 inches (15 cm) of tephra fell in the city of Guadalajara as a result of the 1818 eruption, a figure that is possibly exaggerated! Nevertheless, it is clear from his description that Volcán de Colima figured prominently in the earliest discourse about physical processes of active volcanoes in the scientific literature.

Arguably, the first scientific monitoring of Volcán de Colima was undertaken in 1893–1905 by Diaz (1906), with the support of José María Arreola. During this time period, regular observations of the volcano were made by the Observatorio Meteorológico y Vulcanológico de Zapotlán. Diaz (1906) summarizes these observations in monthly notes and sketches of

activity. At the time, these were among the best scientific records of eruptive activity at any volcano in the world, certainly rivalling the contemporary efforts of Thomas Jaggar (Kilauea, HI, USA) and Giuseppe Mercalli (Vesuvius, Italy). The efforts of Arreola, Diaz and colleagues brought Volcán de Colima more fully to the attention of the international volcano science community and established the volcano as a dominant feature of the Trans-Mexican Volcanic Belt. Their observations also provided important context for understanding of the January 1913 eruption, which impacted a large population then living in the region, especially due to tephra fallout in Ciudad Guzman and nearby areas (Waitz 1936). It clearly demonstrated the potential risks to those living near this massive volcano.

An understanding of the geology of Volcán de Colima and surrounding terrain began to emerge in the mid-twentieth century. Herrera (1967) produced a geological map of the region, followed by regional maps and descriptions by Luhr and Carmichael (1980) and Robin et al. (1987). After the 1980 eruption of Mount St. Helens (WA, USA), a number of groups quickly recognized the prevalence of volcano debris avalanches at Volcán de Colima and Nevado de Colima, identifying debris flow deposits on the south flank of Volcán de Colima (e.g. Luhr and Prestegaard 1988). Further studies have located debris avalanche deposits from the older edifice, Nevado de Colima (Robin et al. 1987; Capra and Macías 2002), and multiple deposits (e.g. Roverato et al. 2011). These studies represent a significant shift in our understanding of the volcanic system, which had been partially biased by the limited range of volcanic activity observed historically. The recognition of volcanic debris avalanches in the stratigraphic record of Volcán de Colima (e.g. Stoopes and Sheridan 1992; Sheridan and Macías 1995; Cortes et al. 2010a) as well as state-of-the-art physical models of the process of flank instability (Borselli et al. 2011) has resulted in significant revision of hazard assessments.

Most recently, mapping of the Colima volcano complex has resulted in a consistent set of chronostratigraphic units and a map that can be readily applied to hazard assessments on a variety of spatial and temporal scales (Cortes et al. 2010b). Important insights into the generation and emplacement of pyroclastic density currents generated at Volcán de Colima from dome and lava flow collapse have been made during detailed field studies, starting with the 1991 eruption (Rodriguez-Elizarraras et al. 1991) up until the recent eruptions (Saucedo et al. 2002; Reyes-Dávila et al. 2016). The hazard maps have recently been updated with the consideration of different eruptive scenarios, ranging from common Vulcanian eruptions and dome-collapse events, through to large VEI 6 Plinian eruptions with possible debris avalanches. Numerical modelling resulted in probabilistic maps, providing the authorities with a range of versatile tools for emergency planning and the construction of effective risk mitigation strategies (Varley et al. 2017). Finally, in the first comprehensive ambient seismic noise tomography analysis, Spica et al. (2017) produce a 3D model of the Volcán de Colima plumbing system providing thought-provoking clues to understand how and where magmas are produced and stored at depth below Volcan de Colima. Their new model remarkably shows a deep, large and well-delineated

elliptic-shape magmatic reservoir below the Colima volcano complex at a depth of about 15 km, in which magma is mainly stored in conduits or inter-fingered dykes as opposed to a horizontally stratified magma reservoir.

Chapters in this volume continue this work of discerning the full range of eruptive activity in this marvellously complex volcanic system. Crummy et al. (Chap. 1) provide new insights into the Holocene tephra stratigraphic record of the volcano, which is key to documenting its history of explosive volcanic eruptions. Norini et al. (Chap. 2) tackle the complex topic of the basement geology of the volcano and the impact of basement faults on the stability of volcano edifices of the Colima Volcano Complex. Cortes et al. (Chap. 3) clarify the stratigraphic record of volcano debris avalanche deposits since the Pliocene, for both Volcán de Colima and Nevado de Colima. Chapters 4, 5 and 6 investigate some of the most profound hazards of the volcano produced by both eruptive and non-eruptive activity: tephra fallout, pyroclastic density currents and lahars. Cumulatively, these chapters document the state of knowledge for a broad range of activities.

In addition to modelling variations in the eruptive style at Volcán de Colima and its eruptive products, a huge effort has been devoted to monitoring of the volcano and to forecasting potential future activity. Geophysical monitoring began in the mid-1970s with the installation of portable seismic networks. This network was made permanent early in the eruption crisis of 1991 (Núñez-Cornú et al. 1994). Varley (Chap. 7) and Arámbula-Mendoza et al. (Chap. 8) describe a dramatic range of integrated monitoring efforts at Volcán de Colima, including seismic, thermal and gas monitoring. These two chapters document a substantial change in monitoring of the volcano over the last 30 years, and demonstrate that it is one of the best monitored volcanoes in North America, largely through the efforts of the Universidad de Colima and its students, along with national and international collaborations. In addition, Varley (Chap. 7) presents a detailed account of the 1998–2015 period.

At the same time as mapping and geophysical studies were underway in the late 1970s, James Luhr and Ian Carmichael, together with colleagues, began to unravel the magmatic history of the volcanic system in detail (e.g. Luhr and Carmichael 1980, 1981, 1990). Fundamentally, they found that the cyclicity in eruptive activity inferred from the eruption record was matched by geochemical cycles, driven by crystal fractionation and magma mixing in the volcano's shallow reservoir. Reubi et al. (Chap. 9) and Lavallée et al. (Chap. 10) expand upon this earlier work, and through the use of new and innovative techniques, provide a 4D view of the magmatic system that is otherwise inaccessible.

In the final chapters of the volume, de la Cruz et al. (Chap. 11) and Rodríguez (Chap. 12) write extremely valuable perspectives on mitigation of risk for those living near the volcano, both by providing long-term probabilistic hazard assessment, and by investigating the social consequences and response to this information. Risk mitigation at the volcano has provided various challenges during recent years, such as the issue of it being located on the border of two states, each with their differences, both in approach and resources.

As with any persistently erupting volcano, it is often difficult to draw the line when reporting details of eruptions. In the case of this volume, the limit is the July 2015 eruption, which proved to be the most important since the last cataclysmic event in 1913. Details of this eruption appear in Chaps. 7 and 8. Between this eruption and the final production of this book, further important activity occurred in 2016 and early 2017. At the end of September 2016, a large batch of magma filled the crater and produced another lava flow, which was emplaced on top of the 2015 flow to the south. The event led to a crisis response, with meetings at national level, increased observational overflights and preparations for evacuations. Notably, the eruption was purely effusive despite a fast ascent rate and evidence of a high volatile content. Large volumes of sulphur dioxide were emitted, which coincided with some heavy rainfall. This produced a considerable fallout of acid rain, producing crop failure or damage at unprecedented levels at this volcano.

Early 2017 featured a series of larger Vulcanian explosions, with the emplacement of a pyroclastic density current in La Arena ravine reaching 4.2 km. Smaller emplacements were observed to the north. Although smaller in magnitude than previous explosions, most notably, those of 2005, they produced an impressive shower of volcanic bombs and in one case, an extraordinary shock wave that rattled windows in the capital Colima as well as cities further afield.

Those of us who have worked in volcano science for many decades recognize the profound changes in our understanding of volcanoes represented by the contributions in this volume. Tremendous advances have occurred, both because of innovative scientific advances and through the hard work of many individuals in the field, laboratory and observatory. We are not finished, as major challenges remain to understand the nature of Volcán de Colima, its activity and potential impacts, while improving our preparedness for the potential future large eruptions. We hope this volume will be useful to scientists engaged in these efforts for many years to come, as well as to the general reader with a profound interest in volcanoes and what we can learn about them. The compilation of state-of-the-art volcano science in this volume will undoubtedly contribute to improve risk perception and societal resilience in the face of volcanic eruptions.

Colima, Mexico — Nick Varley
Tampa, USA — Charles B. Connor
Paris, France — Jean-Christophe Komorowski

References

Arreola, J.M.: Brief notice of observations of Colima. J. Geo. **11**:751–761 (1903)
Arreola, J.M.: Catalogo de las erupciones antiguas del Volcán de Colima, Memorias Soc. Cient A Alzate. **32**:443–481 (1915)
Barcena, M.: Inform sobre el estado actual del Volcán de Colima. Anales Minst. de Formento, Mexico, 385–365 (1887)

Borselli, L., Capra, L., Sarocchi, D., De la Cruz-Reyna, S.: Flank collapse scenarios at Volcán de Colima, Mexico: a relative instability analysis. J. Volcanol. Geotherm. Res. **208**, 51–65 (2011)

Capra, L., Macıas, J.L.: The cohesive Naranjo debris-flow deposit (10 km^3): a dam breakout flow derived from the Pleistocene debris-avalanche deposit of Nevado de Colima Volcano (México). J. Volcanol. Geotherm. Res. **117**(1–2), 213–235 (2002)

Cortes, A., Macias, J.L., Capra, L., Garduño, V.H.: Sector collapse of the SW flank of Volcán de Colima, México. The 3600 yr BP La Lumbre-Los Ganchos debris avalanche and associated debris flows. J. Volcanol. Geotherm. Res. **197**, 52**–**66 (2010a)

Cortés, A., Garduño, V.H., Macías, J.L., Navarro-Ochoa, C., Komorowski, J.C., Saucedo, R., Gavilanes, J.C.: Geologic mapping of the Colima volcanic complex (Mexico) and implications for hazard assessment. Geol. Soc. Am. Spec. Pap. **464**, 249–264 (2010b)

Diaz, S.: Efemerides del Volcán de Colima (1893–1905). Sria. de Formento, Mexico, 168 pp (1906)

Herrera, C.: Geolofia de las Volcanes de Colima. Ph.D. Dissertation, Faculty of Engineering, UNAM (1967)

Luhr, J.F., Carmichael, I.S.: The Colima volcanic complex, Mexico. Contrib. Mineral Petrol. **71**(4), 343–372 (1980)

Luhr, J.F., Carmichael, I.S.: The Colima volcanic complex, Mexico: Part II. Late-quaternary cinder cones. Contrib. Mineral. Petrol. **76**(2), 127–147 (1981)

Luhr, J.F., Carmichael, I.S.:. Petrological monitoring of cyclical eruptive activity at Volcan Colima, Mexico. J. Volcanol. Geotherm. Res. **42**(3), 235–260 (1990)

Luhr, J.F., Prestegaard, K.L.: Caldera formation at Volcán Colima, Mexico, by a large large holocene volcanic debris avalanche. Mexico. J. Volcanol. Geotherm. Res. **35**(4), 335–348 (1988)

Medina Martínez, F.: Analysis of the eruptive history of the Volcán de Colima, Mexico (1560, 1980). Geofísica Internacional, **22**(2) (1983)

Mooser, F.: Catalogue of active Volcanoes of the World, Part XI, 1, "Central America". International Association of Volcanology, Rome 10–13 (1958)

Mooser, F.: Los Volcanes de Colima. Bol. No. 61 del Inst. de Geol. Mexico, 49–61 (1961)

Núñez-Cornú, F., Nava, F.A., De la Cruz-Reyna, S., Jiménez, Z., Valencia, C., García-Arthur, R.; Seismic activity related to the 1991 eruption of Colima Volcano, Mexico. Bull. Volcanol. **56**(3), 228–237 (1994)

Ordoñez, E.: Les Volcans Colima et Ceboruco. Memorias de la Soc. Cient. A Alzate, **11**, 325–333 (1897)

Reyes-Dávila, G., Arámbula-Mendoza, R., Espinasa-Pereña, R., Pankhurst, M.J., Navarro-Ochoa, C., Savov, I., Vargas-Bracamontes, D., Cortés-Cortés, A., Gutiérrez--Martínez, C., Valdés-González, C., Domínguez-Reyes, T., González-Amezcua, M., Martínez-Fierros, A., Ramírez-Vázquez, C.A., Cárdenas-González, L., Castañeda-Bastida, E., Vázquez Espinoza de los Monteros, D., Nieto-Torres, A., Campion, R., Courtois, L., Lee, P.D.: Volcán de Colima dome collapse of July, 2015 and associated pyroclastic density currents, J. Volcanol. Geotherm. Res. **320**, 100–106 (2016)

Robin, C., Mossand, P., Camus, G., Cantagrel, J.-M., Gourgaud, A., Vincent, P.M.: Eruptive history of the Colima volcanic complex (Mexico). J. Volcanol. Geotherm. Res. **31**:99–113 (1987)

Rodríguez-Elizarrarás, S., Siebe, C., Komorowski, J.C., Espíndola, J.M., Saucedo, R.: Field observations of pristine block and ash flow deposits emplaced April 16–17, at Volcán de Colima, Mexico. J. Volcanol. Geotherm. Res. **48**, 399–412 (1991)

Roverato, M., Capra, L., Sulpizio, R., Norini, G.: Stratigraphic reconstruction of two debris avalanche deposits at Colima Volcano (Mexico): insights into pre-failure conditions and climate influence. J. Volcanol. Geotherm. Res. **207**(1–2), 33–46 (2011)

Saucedo, R., Macas, J.L., Bursik, M., Mora, J.C., Gavilanes, J.C., Cortes, A.: Emplacement of pyroclastic flows during the 1998–1999 eruption of Volcan de Colima, Mexico. J. Volcanol. Geotherm. Res. **117**, 129–153 (2002)

Saucedo, R., Macias, J.L., Gavilanes, J.C., Arce, J.L., Komorowski, J.C., Gardner, J.E., Valdez- Moreno, G.: Eyewitness, stratigraphy, chemistry, and eruptive dynamics of the 1913 Plinian eruption of Volcán de Colima, México. J. Volcanol. Geotherm. Res. **191**, 149–166 (2010)

Sheridan, M.F., Macías, J.: Estimation of risk probability for gravity-driven pyroclastic flows at Volcan Colima, Mexico. J. Volcanol. Geotherm. Res. **66**(1–4), 251–256 (1995)

Spica, Z., Perton, M., Legrand, D.: Anatomy of the Colima volcano magmatic system, Mexico. Earth Planet. Sci. Lett. **459**, 1–13 (2017)

Stoopes, G.R., Sheridan, M.F.: Giant debris avalanches from the Colima Volcanic Complex, Mexico: implications for long-runout landslides (>100 km) and hazard assessment. Geology, **20**(4), 299–302 (1992)

Varley, N.R., Cernas, J.A., García, A., López, Z., Meza, M.I.: Riesgos Volcanológicos, Universidad de Colima, Protección Civil del Estado de Colima, Colima (2017)

Waitz, P.: Datos historicos y bibliograficos acera del Volcán de Colima. Memorias de la Soc. Cient. A Alzate, **53**, 349–386 (1936)

Contents

Holocene Eruption History and Magmatic Evolution of the Colima Volcanic Complex

Julia M. Crummy, Ivan P. Savov, Carlos Navarro-Ochoa and Dan J. Morgan

Abstract

The Colima Volcanic Complex (CVC) erupts in both highly explosive and effusive fashion. Detailed radiocarbon dating of tephra fallout deposits exposed in road-cuts on the flanks of Nevado de Colima reveal at least 25 major Plinian eruptions occurred during the last 30,000 years. Deposits from these eruptions are basaltic to andesitic in composition showing an arc affinity in their immobile trace element abundance patterns. Detailed studies of the mineralogy, major and trace element and isotope chemistry reveal two distinct magma types erupted at the CVC during the Holocene. Group I, which comprise the bulk of eruption deposits, are calc-alkaline basaltic-andesites to andesites, while Group II magmas show strong petrological and geochemical similarities to alkaline lamprophyric magmas that formed monogenetic cinder cones to the east and west of the northern CVC. The presence of alkaline and calc-alkaline magmas at the CVC has allowed us to investigate the nature between these magma types in an arc setting. Data presented here reveal that the Group II magmas formed from pulses of alkaline melts intercepting the magmatic storage region of the CVC stratovolcanoes, mixing with the calc-alkaline Group I magmas. These pulses appear to have recurrence rates on the timescales of a few thousand years.

Keywords

Volcan de Colima · Arc magmas · Magmatic evolution · Magma mixing

1 Introduction

Historically, activity at Volcán de Colima is dominantly effusive with rare explosive sub-Plinian to Plinian eruptions, the last of which occurred in January 1913 (Bretón González et al. 2002). However, throughout the late Pleistocene and Holocene, numerous highly explosive eruptions occurred at the CVC, as revealed by tephra deposits exposed on the flanks of Nevado de Colima (Fig. 1; Luhr et al. 2010).

J. M. Crummy (✉)
British Geological Survey, The Lyell Centre, Research Avenue South, Edinburgh EH14 4AP, UK
e-mail: juli@bgs.ac.uk

J. M. Crummy · I. P. Savov · D. J. Morgan
School of Earth and Environment, University of Leeds, Leeds LS2 9JT, UK

C. Navarro-Ochoa
Centro Universitario de Estudios E Investigación En Vulcanología, Universidad de Colima, Colima, Mexico

N. Varley et al. (eds.), *Volcán de Colima*, Active Volcanoes of the World,
https://doi.org/10.1007/978-3-642-25911-1_5

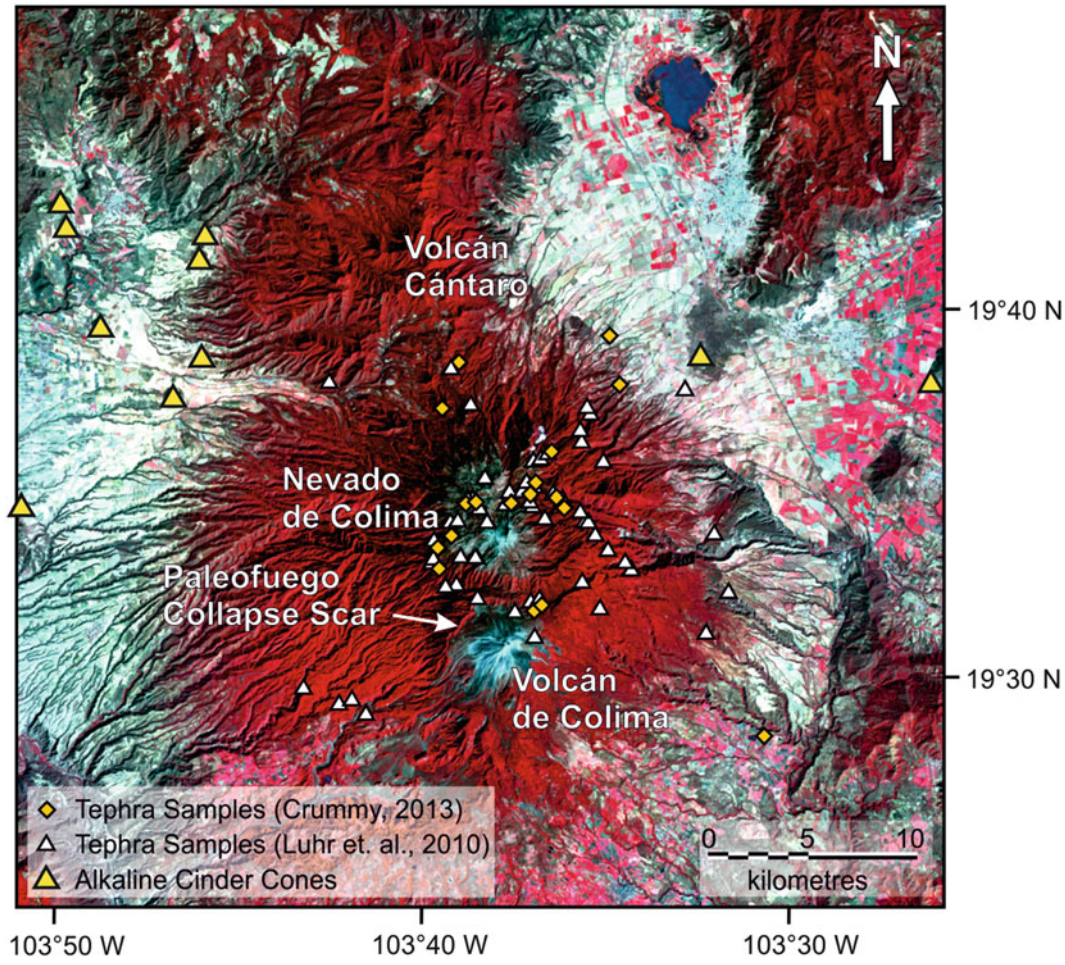

Fig. 1 Sample location map for the Holocene tephra fallout deposits of the CVC. Locations are from new sites sampled in 2010 and 2011 (yellow diamonds; Crummy 2013) and Luhr et al. (2010; white triangles). Also shown are monogenetic cinder cone locations after Luhr and Carmichael (1981) and Carmichael et al. (2006). The majority of samples are located in access roads on the upper slopes of Nevado de Colima. The image is a Landsat image from the United States Geological Survey (USGS). Red areas are forested, pink areas are farmland, and blue areas are unvegetated

Since the 1980s, Volcán de Colima has been the focus of many studies investigating the geochemistry and petrology of the erupted deposits, largely focusing on the current phase of activity and the 1913 eruption (Luhr and Carmichael 1980, 1982, 1990a, b; Medina-Martínez 1983; Robin et al. 1991; Luhr 1993, 2002; Robin and Potrel 1993; Komorowski et al. 1997; Righter 2000; Atlas et al. 2006; Luhr et al. 2006, 2010; Reubi and Blundy 2008; Savov et al. 2008; Saucedo et al. 2010; Verma and Luhr 2010). Based on historical records and petrological and geochemical studies, Luhr (2002) proposed a cycle of ~100 years for explosive Plinian activity at Volcán de Colima.

Much of the work carried out on Volcán de Colima is concerned with forecasting future activity and monitoring current activity (see Varley, this volume); however, few of these studies consider the volcano's explosive past, or patterns of activity which may emerge from a better understanding of the explosive Holocene (and late Pleistocene) eruption deposits. These deposits are largely unstudied and poorly

understood, with few attempts to characterize them: the first by Luhr and Carmichael (1982), and two further more detailed studies by Luhr et al. (2010) and Crummy et al. (2014).

This work incorporates, and expands upon the work of Luhr et al. (2010), focusing on the stratigraphic relationships of the explosive Holocene eruption deposits, and the petrological and geochemical evolution of the erupted magmas during the past 13,000 years. Detailed petrological and geochemical investigations of the erupted tephra fallout deposits presented here reveal a link between the calc-alkaline volcanism responsible for the CVC stratovolcanoes, and alkaline volcanism that formed monogenetic cinder cones to the east and west of the northern CVC. New data, in combination with published and unpublished datasets, are used to investigate the nature of the CVC magmatic plumbing system and the link between alkaline and calc-alkaline volcanism in an arc setting.

2 Volcanic Activity of the CVC

Historical records of activity at Volcán de Colima extend back to 1519 and the arrival of the Spanish conquistadors (Bretón González et al. 2002). Prior to the establishment of volcano observatories in the cities of Colima and Zapotlan in 1898, records of activity are from eyewitness accounts. Bretón González et al. (2002) presented a detailed history of volcanic activity since 1519, summarized here in Fig. 2, in combination with reports from the Smithsonian Institute (Global Volcanism Program 2016). Since 1519, there have been nine highly explosive, VEI = 4 (Volcanic Explosivity Index after Newhall and Self 1982) events, the last of which occurred in 1913. Only the 1818 and 1913 eruptions are well-documented in historical records, with detailed descriptions of thick ash-fall and pyroclastic flows (Bretón González et al. 2002; Luhr 2002). Tephra fallout deposits from these two eruptions are the only historical fallout deposits preserved in the tephra record (Luhr et al. 2010). It is therefore assumed that the 1818 and 1913 events were larger-volume eruptions than the seven other reported VEI = 4 historical events (Fig. 2; Bretón González et al. 2002; Luhr et al. 2010).

The February 1818 Plinian eruption of Volcán de Colima produced a sustained ash column, which resulted in ash-fall in Mexico City ~470 km from the vent, and pyroclastic flows that travelled ~14 km along ravines (Bretón González et al. 2002). For 51 years after the 1818 eruption, activity at Volcán de Colima was restricted to the rise of the magma within the crater, and it was assumed that the volcano was inactive (Luhr and Carmichael 1990b; Bretón González et al. 2002). In January of 1913, Volcán de Colima once again erupted explosively producing a sustained ash column that reached an estimated height of 18–23 km above sea level (a.s.l.) and pyroclastic flows that travelled up to 15 km from the vent (Luhr and Carmichael 1980; Saucedo et al. 2010). For more details of the 1913 Plinian eruption, please refer to Connor et al., this volume. Following the 1913 explosive eruption, the volcano again entered an effusive phase of activity punctuated by small Vulcanian explosions (Robin et al. 1987; Bretón González et al. 2002; Luhr 2002). This type of activity is ongoing at the time of writing (September 2016), and is termed here as interplinian.

2.1 Interplinian Activity

Interplinian deposits are poorly exposed at the CVC having been buried or destroyed by subsequent eruptions; therefore, the nature of such activity is characterized by material erupted between 1869–1909 and 1957–present day. Luhr and Carmichael (1980) were the first to study the Colima andesites, describing the petrology and geochemistry of lava flows and ballistics erupted in 1869, 1913, 1961–1962 and 1975–1976. Further studies on interplinian activity focused on effusive and small explosive (VEI 2–3) deposits erupted between 1961 and 2005 (Robin et al. 1987, 1991; Luhr and Carmichael 1990b; Luhr 1993, 2002; Robin and Potrel 1993; Navarro-Ochoa et al. 2002; Savov et al. 2008).

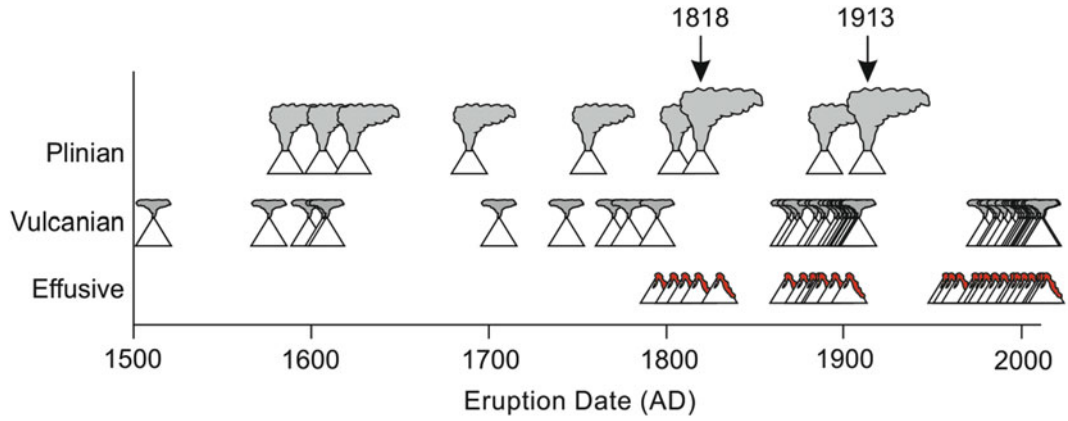

Fig. 2 Schematic diagram summarizing volcanic activity at Volcán de Colima since records began in 1519 using the data from Bretón González et al. (2002) in combination with reports from the Smithsonian Institute (Global Volcanism Program 2016). There is very little information in the records of lava flows from Volcán de Colima, and effusive deposits exposed on the flanks are all post-1818 lava flows (Bretón González et al. 2002). Numerous Vulcanian-type eruptions have occurred throughout historical times and up to nine VEI = 4 eruptions have occurred since the 1500s. Tephra is only preserved from the 1818 and 1913 eruptions and there are numerous eye-witness accounts of these eruptions; therefore, it is assumed that these were larger eruptions than the other seven

In 1869, 51 years after the large explosive 1818 eruption, lava erupted on the northeast side of the Volcán de Colima edifice forming the parasitic cone of Volcancito (Luhr and Carmichael 1990b). Resulting lava flows travelled into the northeast part of the caldera floor and along a ravine to the southeast. Activity continued at Volcancito until 1878 when activity in the main crater resumed (Bretón González et al. 2002). For the next 29 years, Volcán de Colima displayed effusive activity punctuated by small explosive eruptions that produced ash clouds above the vent and block-and-ash flows down the flanks of the volcano (Bretón González et al. 2002). Records of these eruptions are from eye-witness accounts, and no details of column height or flow length were given. From 1904 to 1909 explosive activity decreased and the volcano entered a more fumarolic phase with occasional small explosions (Bretón González et al. 2002).

In 1957, the first activity from the summit of Volcán de Colima since the 1913 eruption was recorded with the extrusion of a new lava dome, followed by the production of lava flows and weak explosions in 1960 and 1961 (Luhr and Carmichael 1980). For the next 30 years, activity was dominated by effusive lava dome extrusion and partial dome collapses, resulting in lava flows reaching up to 4 km in length (Luhr 2002).

A more explosive phase of activity commenced in 1999 with an explosion in February that sent ballistic projectiles up to 3.5 km away from the vent, and in July an eruption that produced an ash column 12 km a.s.l. and pyroclastic flows down the southern flank (Bretón González et al. 2002; Savov et al. 2008; Global Volcanism Program 2016). This explosive phase of activity is continuing at the time of writing (September 2016). For more details of recent activity the reader is referred to Luhr (2002) and Savov et al. (2008), and the chapters of Varley and Reubi et al. in this book.

2.2 Plinian Activity

The tephra fallout deposit of the 1913 explosive eruption blankets Nevado de Colima, varying in thickness from 60 cm (~4 km from the vent) to 6 cm (~10 km from the vent; Luhr et al. 2010; Saucedo et al. 2010; Connor et al., this volume). The 1818 eruption deposit is much thinner and less well-exposed (Luhr et al. 2010). These two units form the top of a stratigraphy comprising

numerous tephra fallout and ash-rich surge deposits resulting from explosive sub-Plinian and Plinian eruptions throughout the Holocene and Late Pleistocene (Fig. 3; Luhr et al. 2010).

During the 1990s and 2000s, Jim Luhr, Carlos Navarro-Ochoa and Ivan Savov sampled and described CVC tephra fallout deposits preserved and exposed on the flanks of Nevado de Colima and in quarries and gullies on the rift floor (Luhr et al. 2010). Through detailed sampling and dating of charcoal found within ash horizons and tephra units, they were able to identify and date at least 25 deposits, erupted between ~30,000 yrs B.P. and the present day (Fig. 3; Luhr et al. 2010). Further field campaigns carried out in January 2010 and February 2011 have built upon the work of Luhr et al. (2010) on the tephrochronology and granulometry of the CVC deposits (Crummy 2013; Crummy et al. 2014). To date, eruption deposits have been described at 89 localities

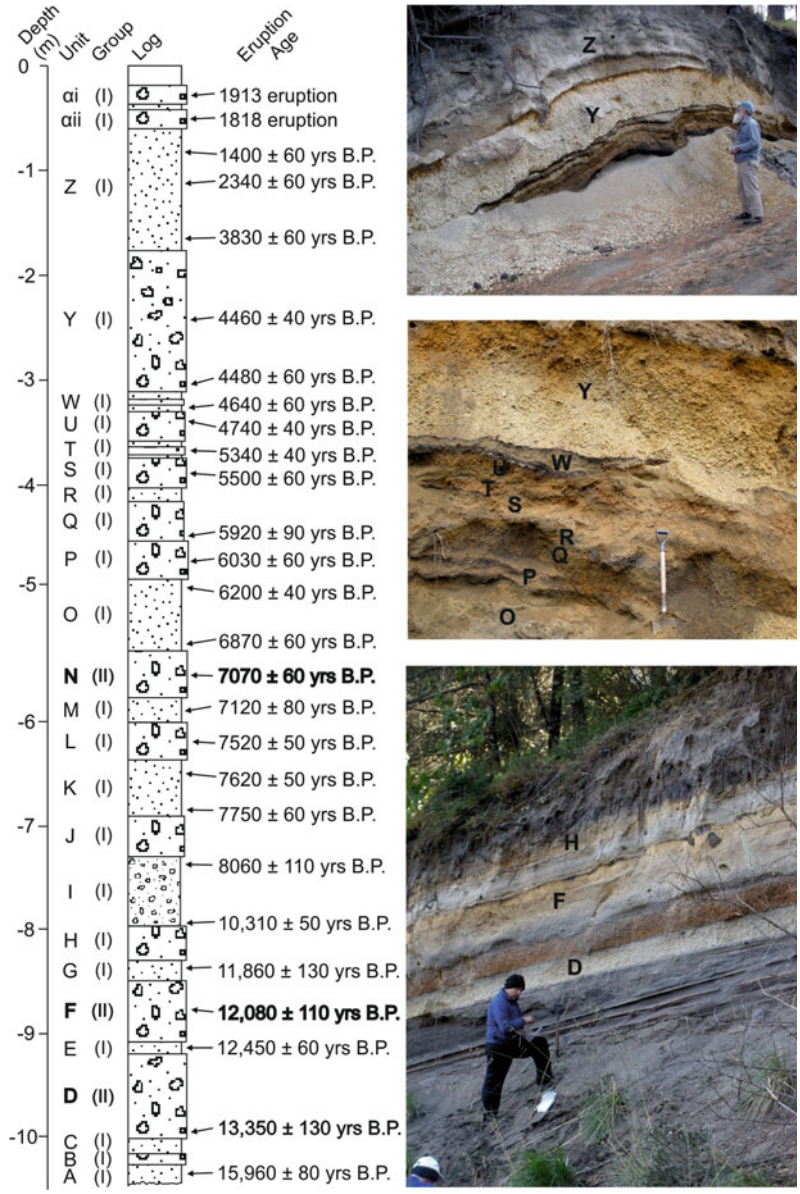

Fig. 3 Composite stratigraphic section and field photographs of deposits resulting from explosive eruptions exposed in road-cuts on the flanks of Nevado de Colima. The unit names and ages are as reported in Luhr et al. (2010). The Group II eruption deposits (units N, F and D) are highlighted in bold

across an area of ~500 km^2, including exposures in quarries on the rift floor (Fig. 1).

In total, 182 radiocarbon ages have been obtained from the CVC eruptive stratigraphy, yielding ages from 80 ± 50 to 29,930 ± 210 yrs B.P. (Fig. 4; Luhr et al. 2010). Of these, 143 ages represent the Holocene (0 to 9000 yrs B.P.). Nevado de Colima is densely vegetated; therefore, the eruption deposits on the volcano's flanks are only exposed in road cuts. Nevado de Colima is a national park which has one main access road on the northeastern flank. Once inside the national park (entrance at 3480 ma.s.l.), there are many more roads. Accordingly, the majority of the tephra deposits are exposed at high elevations, with the older units having been buried or eroded by subsequent eruptions. There are a few roads on the lower slopes; however, the area is prone to landslides and the roads are not maintained.

Using a combination of radiocarbon dating, together with field mapping, petrology and geochemistry (Luhr et al. 2010; Crummy 2013; Crummy et al. 2014), a detailed stratigraphy of the CVC Holocene explosive eruption deposits has been compiled up to 13,000 yrs B.P. (Fig. 3). The field characteristics of the eruption units are given in Table 1.

The stratigraphy of eruption deposits exposed on the flanks of Nevado de Colima comprises tephra fallout deposits varying in thickness from a few centimetres (~10 km from the vent) to over 1 m (~3 km from the vent). The fallout deposits comprise pumice or scoria horizons, with individual clasts varying from <1 to 17 cm. The largest clast sizes are typically found in the most proximal localities, ~3 km from the vent. Angular rock fragments are abundant in all the erupted units, measuring up to 2 cm across (along the long-axis). Interbedded with the tephra layers are ash-rich surge or pyroclastic flow horizons with thicknesses from 2 cm to over 1 m. These ash beds are typically rich in charcoal fragments, and commonly contain reworked pumice and scoria from underlying tephra fallout deposits.

2.3 Monogenetic Cinder Cones

To the east and west of the extinct Volcán Cántaro, located to the north of Nevado de

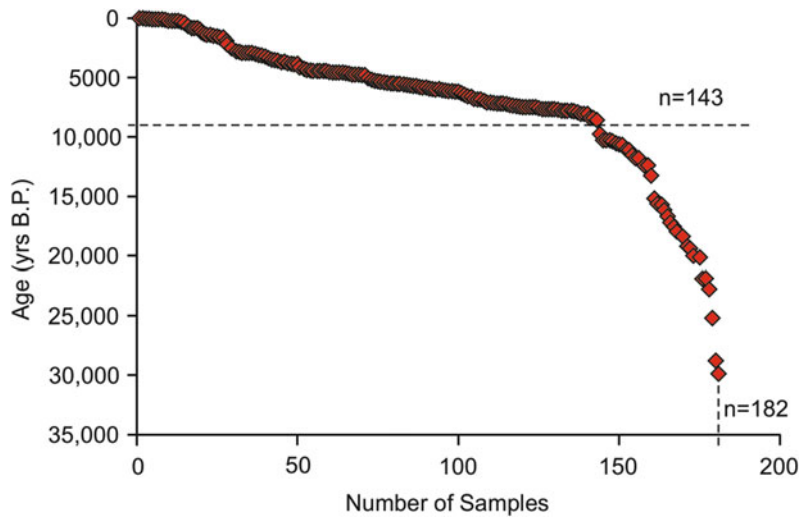

Fig. 4 Radiocarbon ^{14}C ages for the explosive Plinian CVC eruption deposits (Komorowski et al. 1997; Luhr et al. 2010). Out of a total of 182 dates, 143 of these were sampled between 9000 yrs B.P. and present. The younger eruption deposits are well exposed high on the flanks of Nevado de Colima, while the older eruption deposits are less well exposed, confined to lower elevations where the slopes are densely vegetated and access is difficult

Table 1 Field characteristics of CVC tephra fallout deposits discussed in the text

Unit	Eruption age (yrs B.P.)	Group	Color (dry)	Thickness (cm)	Max. pumice size (cm)	Max. lithic size (cm)	Sorting	Composition
Y	4460 ± 40	I	Cream	48–140	17	7	Inverse	Andesite
W	4480 ± 60–4540 ± 60	I	Dark brown	8–28	6	5	Normal	Basaltic-andesite
U	4740 ± 40–4760 ± 70	I	Dark orange	15–20	4	2	Normal	Basalt/basaltic-andesite
S	5430 ± 50–5500 ± 60	I	Dark brown-orange	12–46	4.5	2	Normal	Basaltic-andesite
P	5980 ± 50–6150 ± 40	I	Cream	6–40	9	6	Normal	Basaltic-andesite
N	6950 ± 50–7070 ± 60	II	Orange	12–60	12	2	Normal	Basaltic-andesite
L	7520 ± 50–7530 ± 80	I	Dark brown	4–50	6	3	Inverse	Andesite
J	7750 ± 60–7760 ± 50	I	Pale orange-cream	7–15	6	3	Inverse	Andesite
H	9770 ± 60–10,310 ± 50	I	Dark grey	15–42	5	2	Inverse	Basaltic-andesite
F	11,840 ± 70–12,080 ± 150	II	Grey	30–90	5	8	Normal	Basalt
D	12,460 ± 60–13,350 ± 130	II	Grey	32–180	4.5	3	Inverse	Basalt

Eruption ages are from radiocarbon ^{14}C dating of charcoal found within or between tephra fallout deposits (Komorowski et al. 1997; Luhr et al. 2010). Maximum lithic fragment and pumice clast sizes are found in sections 4–5 km from the currently active vent

Colima and where volcanic activity at the CVC began approximately 1.7 Ma (Luhr and Carmichael 1990a), eleven cinder cones erupted on the rift floor between 1.2 Ma and 62 ka (Fig. 1; Luhr and Carmichael 1981; Allan and Carmichael 1984; Carmichael et al. 2006). The two oldest cones erupted at 1.2 and 0.5 Ma, producing <0.003 km^3 of calc-alkaline basalt and basaltic-andesite (Luhr and Carmichael 1981; Allan and Carmichael 1984; Carmichael et al. 2006). Nine of the cinder cones are alkaline, producing ~1.3 km^3 magma between 450 and 62 ka (Luhr and Carmichael 1981; Allan and Carmichael 1984; Carmichael et al. 2006). The majority of the alkaline mafic magmas (>99%) erupted between 240 and 60 ka (Carmichael et al. 2006). During this time, calc-alkaline volcanism had migrated south from Volcán Cántaro and was ongoing at the Nevado de Colima volcano (Robin et al. 1987; Luhr and Carmichael 1990a; Cortés et al. 2005, 2010).

The alkaline cinder cones were first described by Luhr and Carmichael (1981), who classified them as primitive basanites to minette lamprophyres with 47.6–50.3 wt% SiO_2, 7.4–15.3 wt% MgO and 2.5–4.4 wt% K_2O. The occurrence and source of the alkaline magmas is discussed in detail in the geological literature (Luhr and Carmichael 1981; Wallace and Carmichael 1989; Lange and Carmichael 1990; Luhr 1997; Carmichael et al. 2006; Maria and Luhr 2008; Vigouroux et al. 2008; Cai 2009); however, the relationship between the calc-alkaline and the alkaline magmas remains poorly understood.

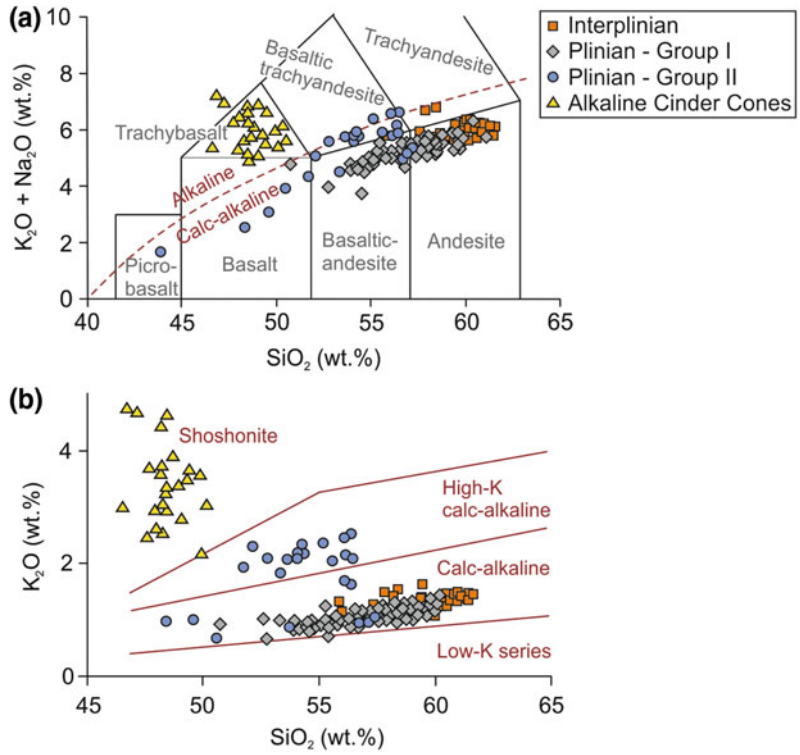

Fig. 5 Classification of the CVC eruption deposits. **a** Total alkalis-silica (TAS) classification diagram after Le Maitre et al. (2002) for CVC interplinian and Plinian eruption deposits and the alkaline cinder cone magmas. The dashed line separating the alkaline from calc-alkaline fields is after Irvine and Baragar (1971). **b** K_2O versus SiO_2 classification diagram after Le Maitre et al. (2002). Data sources for the interplinian and Plinian deposits are given in the text. Plinian tephra fall deposits range in composition from picro-basalt to andesite. Interplinian deposits are typically andesitic in composition. The alkaline cinder cone magmas are high-K shoshonites (Luhr and Carmichael 1981; Carmichael et al. 2006; Maria and Luhr 2008; Vigouroux et al. 2008; Cai 2009)

3 Mineralogy of Erupted Deposits

The majority of CVC eruptive products are basaltic-andesite to andesite in composition (Fig. 5) with the typical mineral assemblage of plagioclase + orthopyroxene + clinopyroxene + hornblende + Fe–Ti oxides ± olivine (Luhr and Carmichael 1980, 1982; Savov et al. 2008; Luhr et al. 2010). Olivine phenocrysts are typically present only in the most mafic units.

The interplinian lavas are typically highly crystalline and have up to 52 vol% crystals comprising the aforementioned mineral phases (Luhr and Carmichael 1980). The groundmass is also highly crystalline, comprising glass and a mesostasis of the same minerals, with the exception of hornblende, which is not found in the groundmass (Luhr and Carmichael 1980). Xenocrystic olivine displaying pyroxene and oxide overgrowths occur in many samples (Luhr and Carmichael 1980). Hornblende phenocrysts all display disequilibrium with breakdown rims of pyroxene and Fe–Ti oxides (Luhr and Carmichael 1980, 1990b; Luhr 2002; Savov et al. 2008).

The bulk of the tephra fallout deposits exposed in road-cuts comprise pumice and scoria clasts with 10–25 vol% phenocrysts and microphenocrysts of the above mineral phases. The groundmass comprises highly vesiculated intermediate to felsic glass (54–74 wt% SiO_2) with abundant microlites of the same mineral phases with the exception of hornblende. Plagioclase, orthopyroxene and clinopyroxene

phenocrysts all display complex zoning patterns interpreted to represent multiple magma recharge events (Crummy et al. 2014).

Three of the tephra fallout deposits, units N, F and D of the Luhr et al. (2010) stratigraphy, which erupted c. 7000, c. 12,000 and c. 13,000 yrs B.P. (Fig. 3), are mineralogically distinct from the rest of the CVC tephra deposits. Samples from these units have low crystallinity (10–15 vol%) comprising phenocrysts and microphenocrysts of plagioclase + clinopyroxene + olivine + hornblende + phlogopite + Fe–Ti oxides + orthopyroxene. The groundmass comprises highly vesiculated, dark, mafic to felsic glass (49.5–66.9 wt% SiO_2) with abundant microlite crystal phases dominated by plagioclase and clinopyroxene.

Based on the mineralogy and whole-rock geochemistry (see below), the explosive eruption deposits have been divided into two groups. Group I comprises the bulk of the tephra units, while Group II comprises the three distinct (phlogopite-containing) tephra units N, F and D (see Table 2).

Each of the three units that make up the Group II eruption deposits have phlogopite phenocrysts and/or microphenocrysts, which are not present in scoria and pumice from the Group I deposits. The Group II units are, however, mineralogically distinct from each other (Table 2). Unit N scoria phenocrysts comprise predominantly plagioclase and clinopyroxene, with up to 1 vol% olivine, and trace abundances of hornblende and phlogopite. Scoria from unit F has a lower crystallinity when compared with units N and D, and the mineral assemblage is dominated by clinopyroxene, olivine and phlogopite with up to 1 vol% plagioclase and trace hornblende. Unit D scoria has the highest crystallinity, comprising predominantly hornblende and plagioclase, with clinopyroxene and up to 1 vol% olivine and phlogopite. The groundmass also appears to be more crystalline in unit D, with abundant microlites. Fe–Ti oxides are present in all samples from 1 to 3 vol%, and are most abundant in unit D. As observed within the Group I tephra samples, plagioclase and clinopyroxene phenocrysts from Group II scoria reveal crystallization histories involving complex magma recharge and mixing events (Crummy et al. 2014). For more detailed descriptions of the mineralogy of the Colima calc-alkaline tephra, the reader is referred to Crummy et al. (2014).

Table 2 Mineralogy of pumice and scoria from the CVC Plinian tephra fallout deposits

Unit	Group	Crystallinity (vol%)	Plag (vol%)	Cpx (vol%)	Opx (vol%)	Hbd (vol%)	Olivine (vol%)	Phlog (vol%)	Fe–Ti oxides (vol%)
Y	I	6–10	3–5	0–trace	0–trace	2–4	–	–	Trace–1
W	I	13–19	7–10	1–2	1–3	2–5	Trace–1	–	1
U	I	20–25	12–15	1–2	3–4	2–5	1–2	–	1
S	I	12–17	7–10	1	1–2	1–3	1–2	–	1
P	I	14–22	10–15	1–2	1–3	Trace	Trace	–	1
N	II	9–13	5–10	1–2	Trace	Trace	Trace–1	Trace	1
L	I	11–19	5–10	Trace	1	3–5	–	–	1–2
J	I	11–16	7–10	1	1–2	1	–	–	1–2
H	I	13–17	2–10	1–2	2–3	Trace–5	Trace–2	–	1
F	II	7–12	Trace–1	2–5	–	Trace	1–3	1–2	1–2
D	II	10–15	1–3	Trace–2	Trace	3–7	Trace–1	0–1	1–3

The three units that comprise Group II contain lower abundances of plagioclase and contain phlogopite. The mineral proportions are given as volume % of the whole sample, and were estimated from thin sections on the optical microscope

Plag plagioclase; *Opx* orthopyroxene; *Cpx* clinopyroxene; *Hbd* hornblende; *Phlog* phlogopite

The alkaline cinder cones were described by Luhr and Carmichael (1981) as forming a transitional series from basanite to minette based on the appearance and increasing abundance of phlogopite, sanidine, leucite and apatite. The typical mineral assemblage of the basanites, as defined by Luhr and Carmichael (1981), comprises phenocrysts and microphenocrysts of olivine + clinopyroxene + plagioclase (labradorite $An_{50–70}$) + microphenocrysts of titanomagnetite. Leucite-basanites have the characteristic mineral assemblage of olivine + clinopyroxene phenocrysts, and microphenocrysts of sanidine + leucite + titanomagnetite + apatite + phlogopite (Luhr and Carmichael 1981). The minettes comprise phenocrysts of olivine + clinopyroxene + phlogopite + apatite and microphenocrysts of sanidine, leucite, titanomagnetite, apatite and phlogopite (Luhr and Carmichael 1981).

4 Whole-Rock Geochemistry

A database of whole-rock major and trace elements for the CVC has been compiled from newly collected data (Crummy 2013), as well as from the CVC literature (Luhr and Carmichael 1980, 1981, 1982; Allan and Carmichael 1984; Robin et al. 1991; Luhr 1993, 2002; Robin and Potrel 1993; Komorowski et al. 1997; Carmichael et al. 2006; Maria and Luhr 2008; Savov et al. 2008; Vigouroux et al. 2008; Cai 2009; Luhr et al. 2010; Saucedo et al. 2010) and unpublished data obtained by James Luhr and Ivan Savov. The full database comprises 398 samples from the CVC, including the alkaline cinder cones; of these 252 are from the Holocene and late Pleistocene explosive tephra deposits. The ranges of major element composition for the Group I and Group II eruption deposits are listed in Table 3.

4.1 Major Elements

The CVC eruptive products show a wide range in composition from basalt to andesite based on the Total-Alkalis Silica (TAS) and K_2O versus SiO_2 diagrams of Le Maitre et al. (2002; Fig. 5). The majority of the deposits are calc-alkaline; however, some samples appear to be trending towards the high-K alkaline cinder cone compositions.

The geochemical evolution of the CVC eruption deposits is shown on time series plots

Table 3 Ranges of major element concentrations in weight % for the Group I and Group II calc-alkaline basalts to high silica andesites

Unit	SiO_2	TiO_2	Al_2O_3	FeOt	MnO	MgO	CaO	Na_2O	K_2O	P_2O_5
Y	53.9–60.4	0.4–0.7	17.9–21.5	4.7–5.8	0.10–0.11	1.8–2.8	5.0–5.9	3.8–4.9	1.0–1.5	0.17–0.31
W	54.7–57.1	0.6–0.8	17.7–18.9	5.7–6.6	0.11–0.12	3.9–5.9	6.4–7.5	3.8–4.4	0.8–1.1	0.20–0.21
U	50.7–57.8	0.5–0.8	17.4–21.4	5.6–7.0	0.10–0.12	2.3–6.1	5.5–7.5	3.3–4.4	0.7–1.3	0.19–0.35
S	54.6–58.6	0.5–0.8	17.1–19.1	4.8–6.5	0.09–0.12	3.6–5.8	5.7–7.5	4.0–4.4	0.9–1.3	0.17–0.15
P	55.4–59.7	0.5–0.8	17.2–19.6	4.7–5.8	0.08–0.11	2.6–6.2	5.6–7.1	4.0–4.7	1.0–1.3	0.16–0.22
N	**52.8–56.5**	**0.8–0.9**	**16.3–18.8**	**5.9–6.0**	**0.11–0.11**	**3.3–6.2**	**5.7–7.2**	**3.5–4.2**	**1.6–2.5**	**0.28–0.56**
L	58.0–59.9	0.6–0.7	16.9–17.8	4.9–5.4	0.09–0.10	3.9–5.1	5.9–6.3	4.2–4.7	1.0–1.2	0.15–0.18
J	53.4–59.5	0.6–1.0	16.4–17.5	5.2–7.0	0.10–0.12	4.6–6.0	5.9–8.1	3.6–4.7	1.1–1.9	0.15–0.39
H	54.5–58.7	0.7–0.9	15.7–18.0	5.8–7.2	0.11–0.13	4.0–7.3	6.7–8.0	2.9–4.4	0.8–1.1	0.13–0.50
F	**43.9–53.3**	**0.8–1.3**	**14.4–19.2**	**6.9–9.1**	**0.09–0.13**	**6.4–8.1**	**6.9–8.0**	**1.3–3.5**	**0.4–3.5**	**0.27–0.68**
D	**53.7–57.5**	**0.8–0.9**	**15.9–18.6**	**6.2–6.9**	**0.11–0.13**	**2.8–6.1**	**6.4–8.0**	**3.4–4.4**	**1.0–2.2**	**0.21–0.51**

Data are from Luhr and Carmichael (1981, 1982) and Luhr et al. (2010) and unpublished data collected by Ivan Savov and Jim Luhr related to the Holocene tephra fallout deposits, and by Julia Crummy as part of her Ph.D. thesis at the University of Leeds (Crummy 2013)
The Group II units are in bold

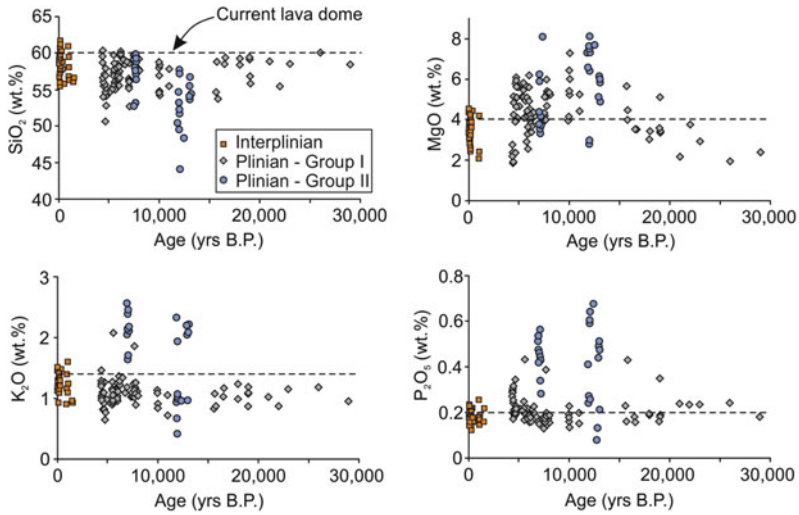

Fig. 6 Time series plots showing the variations in whole-rock major element geochemistry for the CVC eruption deposits over the past 30,000 years. Also shown is the composition of the current lava dome (2007–2010; unpublished dataset). The deposits are divided into two groups based on the geochemical distinctions; the deposits with high MgO, K_2O and P_2O_5 form Group II (blue circles)

(Fig. 6). The interplinian eruption deposits show little variation in whole-rock major element geochemistry, while the explosive (Plinian) eruption deposits show a wide variation in SiO_2, MgO, K_2O and P_2O_5. Overall the MgO content appears to increase from 30,000 yrs B.P. to 12,000 yrs B.P., and then decreases from ~10,000 yrs B.P. to the present. This pattern is somewhat reflected in the SiO_2 content, which shows increases in the same samples that show lower MgO (in the last 10,000 yrs). However, there are fewer samples from 10,000 to 30,000 yrs B.P., so it is difficult to draw concrete conclusions from the available dataset.

The variations of K_2O and P_2O_5 with time reveal the majority of the eruption deposits show little compositional variation; however, the Group II samples, which erupted c.7000, c.12,000 and c.13,000 yrs B.P., display distinctly high K_2O and P_2O_5 (Fig. 6).

The Group I tephra which, in terms of composition, incorporate the interplinian products, are calc-alkaline basaltic-andesites to high silica andesites with SiO_2 contents ranging from 50.7 to 60.3 wt% (Fig. 5). Overall the whole-rock major element systematics show an evolutionary trend toward increasing K_2O and Na_2O and decreasing MgO, CaO, FeOt, TiO_2, MnO and P_2O_5 with increasing SiO_2 (Fig. 7). These trends are consistent with evolution from a mafic magma parent, where the crystallization of the ferromagnesian minerals olivine, orthopyroxene, clinopyroxene and hornblende, and the Ca-rich plagioclase, leave residual melts that are more and more depleted in MgO, CaO, FeOt, TiO_2, MnO, while increasing their SiO_2 and alkalis.

The Group II units are more mafic than the Group I deposits, comprising basalt to basaltic-andesite with SiO_2 contents ranging from 43.9 to 57.5 wt% (Fig. 5). Overall, the Group II eruption deposits follow a similar differentiation trend to the Group I calc-alkaline series, with increasing K_2O and Na_2O and decreasing MgO, CaO, FeOt, MnO and P_2O_5 with increasing SiO_2 (Fig. 7). However, the Group II eruption deposits are geochemically distinct, with elevated K_2O (up to 3.5 wt%) and P_2O_5 (up to 0.68 wt%) relative to the Group I tephra (Figs. 6 and 7).

Figure 8 shows SiO_2 versus MgO and SiO_2 versus K_2O variation diagrams for Group II tephra with the main mineral phases determined via electron microprobe analyses (Crummy 2013). As minerals crystallize from a mafic parent melt, the composition of the melt is driven away from the

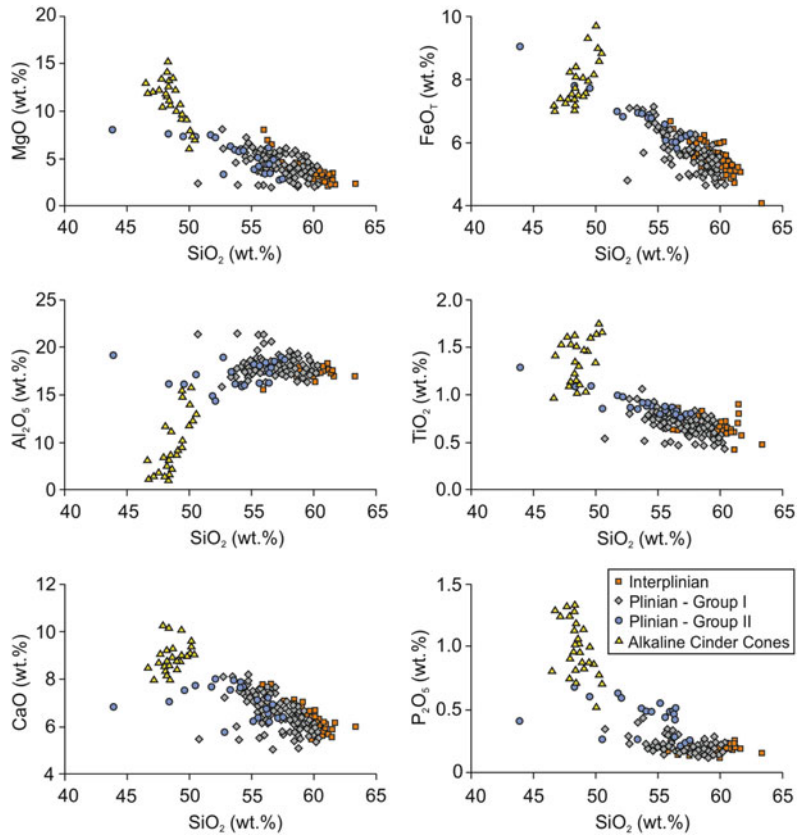

Fig. 7 Whole-rock major element variation diagrams for interplinian and Plinian eruption deposits of the CVC. Also plotted are whole-rock major element compositions for the alkaline cinder cones (Luhr and Carmichael 1981; Carmichael et al. 2006; Maria and Luhr 2008; Vigouroux et al. 2008; Cai 2009). The interplinian deposits are typically more evolved with higher SiO_2 and Al_2O_3, and lower MgO, FeOt, TiO_2, CaO and P_2O_5 contents relative to the Plinian deposits

composition of the extracted mineral assemblage, towards higher SiO_2 and K_2O and lower MgO concentrations. By projecting the differentiation trend back from the groundmass glass composition, through the parental melt composition, it is possible to determine the extracted mineral assemblage. The Group I magmas follow a trend defined by the extraction of plagioclase + hornblende + clinopyroxene + orthopyroxene (Fig. 8). The trend towards high K_2O and low MgO with increasing SiO_2 displayed by the Group II eruption deposits could be explained by the fractionation of plagioclase + phlogopite + clinopyroxene + orthopyroxene + olivine + hornblende from a mafic parent melt. However, not all Group II samples follow this trend. For example, some of the tephra samples from unit D follow the differentiation trend displayed by the Group I eruption deposits, while others lie along the Group II fractionation trend (Fig. 8). Similar variations are observed in the unit N and F samples, with many lying off the differentiation trends. These variation diagrams therefore reveal that not all the Group II samples can be linked to the Group I magmas through simple fractional crystallization from a common mafic parent. Accordingly, the wide range of K_2O (and P_2O_5, CaO, Al_2O_3) within the Group II units suggests a magma mixing process between two compositionally distinct magma batches.

The alkaline cinder cone deposits are characterized by low SiO_2 and Al_2O_3, and high TiO_2, MnO, MgO, CaO, K_2O and P_2O_5 (Fig. 7). These magmatic rocks show relatively little variation in SiO_2 content (47.6–50.3 wt%), but show large variations in MgO (7.4–15.3 wt%), K_2O (2.5–4.4 wt%) and P_2O_5 (0.7–1.3 wt%). The high MgO, K_2O and P_2O_5 contents are reflected in their mineralogy, with assemblages dominated by mafic minerals, and the presence of phlogopite, sanidine and apatite phenocrysts and microphenocrysts (Luhr and Carmichael 1981).

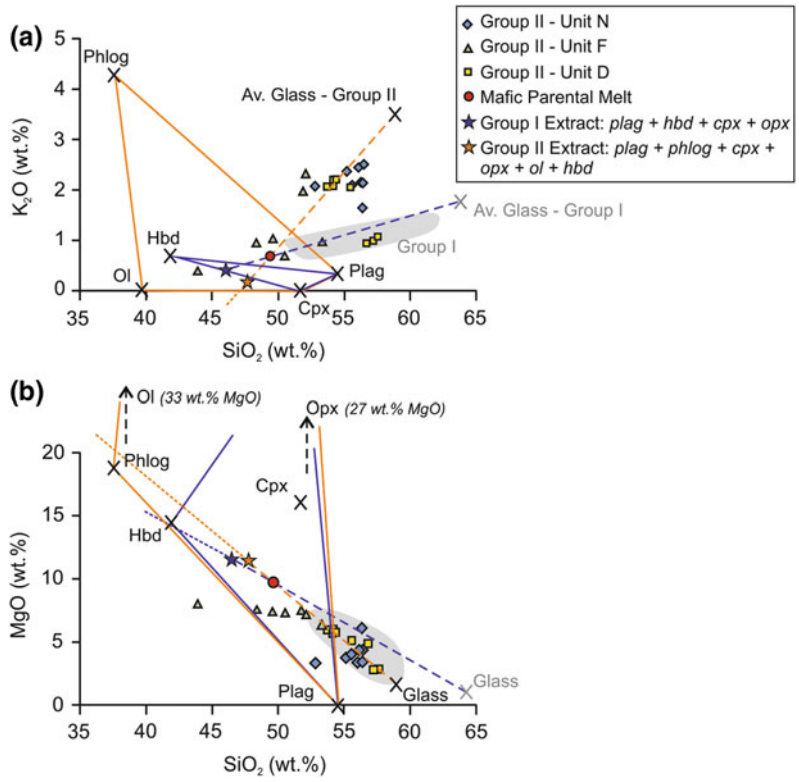

Fig. 8 K_2O and MgO variation with SiO_2 showing the control of the main mineral phases on the chemical trends. Projecting the melt composition from the groundmass glass back through the parental melt reveals the fractionating mineral assemblage driving magma differentiation. Sample SAY-22E from a basaltic cinder cone east of the CVC is used to represent the parental melt composition (Luhr and Carmichael 1981; Luhr 1997; Verma and Luhr 2010). The Group I samples follow a trend of increasing K_2O (**a**) and decreasing MgO (**b**) with increasing SiO_2 reflecting the extraction of plagioclase (plag) + hornblende (hbd) + orthopyroxene (opx) + clinopyroxene (cpx) [+olivine] from a mafic parental melt. The Group II eruption deposits reveal variations that cannot be explained by fractional crystallization alone. Some of the Group II samples follow the Group I trend; however, some samples from the same eruption unit follow a trend reflecting the extraction of plagioclase + phlogopite (phlog) + clinopyroxene + orthopyroxene + olivine (ol) + hornblende, and some do not appear to follow any fractionation trend

The alkaline cinder cones form a distinct group that lies off the calc-alkaline magma differentiation trend indicating a separate source composition and subsequent fractionation trends (Figs. 5 and 7).

4.2 Trace Elements

Incompatible trace element abundance patterns in the Group I and Group II CVC eruption deposits are consistent with those typical of subduction-related magmas (Fig. 9a; Pearce 1982; Straub et al. 2010 and references therein). All CVC tephra samples show enrichments in large ion lithophile elements (LILE: Rb, Ba, Th, and K) relative to high field strength elements (HFSE: Nb, Ta, Ti, Hf, Zr,) attributed to the addition of slab-derived fluids/melts to depleted mantle wedge sources (Vigouroux et al. 2008 and references therein). The relative depletions in the HFSE reflect the presence of stable mineral phases in the subducting slab or mantle wedge, such as ilmenite, titanite, rutile, zircon, apatite and garnet (Pearce 1982). The Group II samples display stronger enrichments in the incompatible

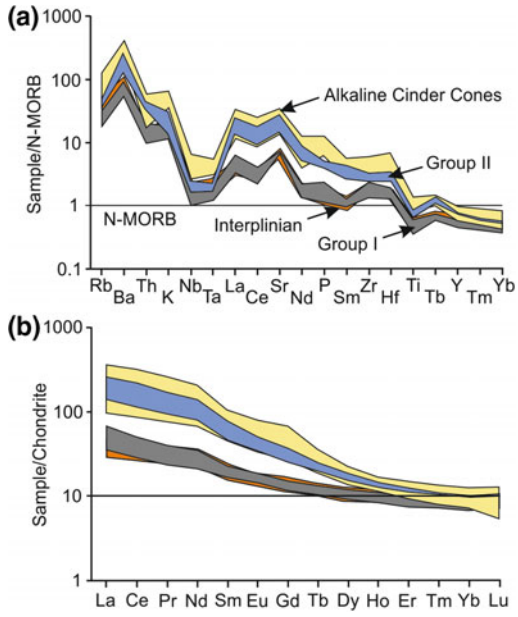

Fig. 9 Incompatible whole-rock trace element abundances normalized to N-MORB and REE normalized to Chondrite for the CVC eruption deposits. Normalizing values are from Sun and McDonough (1989) and Nakamura (1974), respectively. All the CVC eruption deposits, including the alkaline cinder cones, have subduction-related trace element abundance patterns characterized by depletions in the HFSE (Ta, Nb) relative to the LILE (Rb, Ba, K). The interplinian and Group I Plinian samples have overlapping compositions, while the Group II samples show stronger enrichments in all the incompatible trace elements, partially overlapping the alkaline cinder cone compositions

trace elements relative to the Group I units, and partially overlap the alkaline magma compositions (Fig. 9a).

Chondrite-normalized rare earth element (REE) abundance patterns in CVC magmas reveal that the light REE (La to Nd) are always enriched relative to the middle REE and heavy REE (Sm to Lu; Fig. 9b), reflecting a control of amphibole, clinopyroxene and garnet in the mantle source (Hanson 1980). Again, the abundances of the REE in the Group II eruption deposits overlap the abundances in the alkaline cinder cone magmas. These show very high light REE abundances (Fig. 9b), possibly reflecting lower degrees of partial melting (Hanson 1980).

4.3 Sr–Nd Isotopic Compositions

The radiogenic isotopic composition of a magma is inherited from its source during partial melting and remains unchanged as fractional crystallization progresses in the absence of contamination by an isotopically distinct component (Faure and Mensing 2005). However, isotopic variations will occur if, during ascent, the magma interacts with other batches of previously formed magma or crystalline mush, or assimilates wall-rocks or basement lithologies with isotopically distinct compositions (Hawkesworth and van Calsteren 1984; Faure and Mensing 2005). Accordingly, the $^{87}Sr/^{86}Sr$ and $^{143}Nd/^{144}Nd$ isotopic ratios have been widely used to fingerprint magma source(s) and identify open- and closed-system processes occurring in the magma storage region such as magma mixing, crustal assimilation and fractional crystallization (AFC; e.g. Kempton et al. 1991; Tatsumi et al. 1992; Straub et al. 2010; Verma and Luhr 2010; Schmidt and Grunder 2011).

Within Group I eruption deposits, $^{87}Sr/^{86}Sr$ and $^{143}Nd/^{144}Nd$ show a narrow range, varying from 0.70338 to 0.70371 and 0.51290 to 0.51295, respectively (Table 4; Fig. 10). The Group II units display slightly higher $^{87}Sr/^{86}Sr$ and lower $^{143}Nd/^{144}Nd$ than the majority of the Group I samples. Tephra units N and D display a narrow range in $^{87}Sr/^{86}Sr$ and $^{143}Nd/^{144}Nd$, varying from 0.70365 to 0.70372 and 0.51291 to 0.51294, respectively (Fig. 10). Unit F displays a much wider range in $^{87}Sr/^{86}Sr$ (0.70358–0.70408) and $^{143}Nd/^{144}Nd$ (0.51279–0.51293). However, there is a clear distinction within unit F samples; two of the samples have more radiogenic $^{87}Sr/^{86}Sr$ and less radiogenic $^{143}Nd/^{144}Nd$ corresponding with their lower SiO_2 content (Fig. 10a, b). The clear separation of these two samples from the rest of the Group II eruption deposits suggests either a separate source, or contamination from a magma or crystalline mush with high $^{87}Sr/^{86}Sr$ and low $^{143}Nd/^{144}Nd$ values. The relatively flat trend displayed by the Group I and the majority of the Group II samples suggest fractional crystallization from a homogenous melt.

Table 4 $^{87}Sr/^{86}Sr$ and $^{143}Nd/^{144}Nd$ isotope ratio compositions for the Group I and Group II eruption deposits

Sample	Unit	$^{87}Sr/^{86}Sr$	2σ error ($\times 10^{-6}$)	$^{143}Nd/^{144}Nd$	2σ error ($\times 10^{-6}$)
VF95-09X	Y	0.703627	±4	0.512940	±11
VF97-06D	Y	0.703633	±6	0.512912	±4
VF97-13B	Y	0.703623	±6	0.512916	±6
VF98-02W	W	0.703582	±4	0.512916	±6
VF95-06W	W	0.703574	±6	0.512941	±8
VF10-01U	U	0.703586	±4	0.512924	±6
VF10-02U	U	0.703593	±4	0.512932	±6
VF10-04U	U	0.703635	±5	0.512921	±7
VF10-07U	U	0.703594	±4	0.512934	±4
VF95-06P	S	0.703555	±4	0.512953	±3
VF95-09T	S	0.703592	±4	0.512932	±6
VF10-03Q	P	0.703577	±13	0.512948	±5
VF10-07M3	P	0.703604	±4	0.512927	±5
VF10-01P	P	0.703564	±4	0.512948	±7
VF10-03Pi	P	0.703557	±10	0.512902	±7
VF10-07D	**N**	**0.703723**	**±3**	**0.512908**	**±6**
VF95-09G	**N**	**0.703711**	**±4**	**0.512916**	**±4**
VF10-03N	**N**	**0.703710**	**±5**	**0.512922**	**±4**
VF95-09E	L	0.703597	±3	0.512909	±5
VF10-03M2	L	0.703604	±4	0.512932	±8
VF10-03L	J	0.703610	±4	0.512937	±6
VF00-06R	H	0.703384	±3	0.512952	±5
VF94-06E	H	0.703705	±5	0.512913	±5
VF97-01Di	H	0.703689	±5	0.512913	±5
VF95-06E	**F**	**0.703576**	**±4**	**0.512927**	**±10**
VF01-02Ps	**F**	**0.704084**	**±4**	**0.512791**	**±4**
VF01-05PA	**F**	**0.704044**	**±4**	**0.512787**	**±5**
VF10-04F	**F**	**0.703681**	**±4**	**0.512913**	**±5**
VF95-01B	**D**	**0.703645**	**±5**	**0.512936**	**±5**
VF01-02Ni	**D**	**0.703696**	**±4**	**0.512920**	**±10**
VF01-05N	**D**	**0.703695**	**±4**	**0.512908**	**±5**

Values are reported to 2σ error on the 6th decimal digit, and have been normalized to the NBS-987 and La Jolla standards for Sr and Nd, respectively

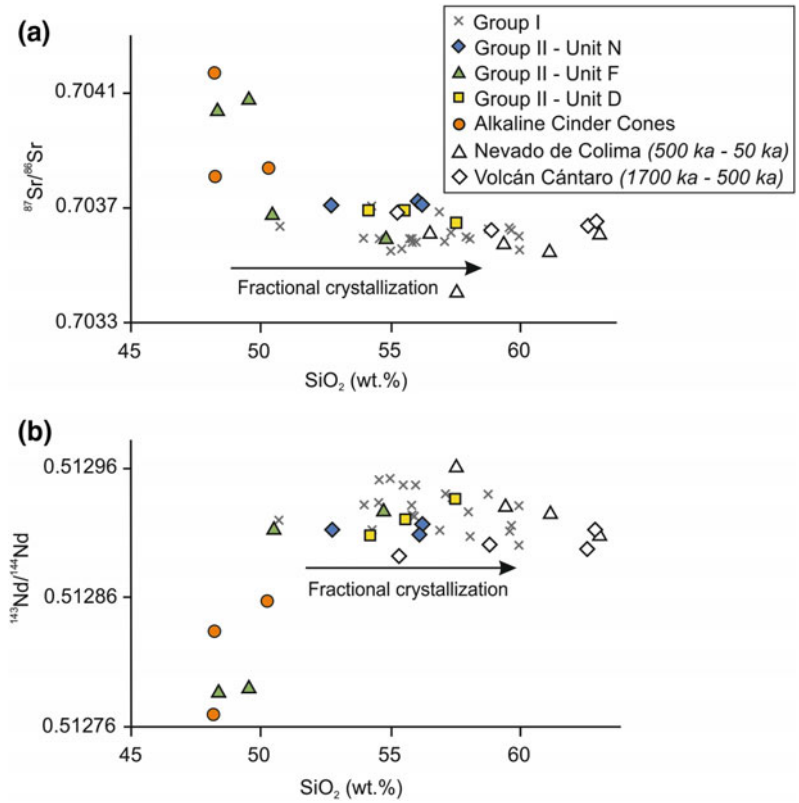

Fig. 10 $^{87}Sr/^{86}Sr$ and $^{143}Nd/^{144}Nd$ variation with SiO_2 for the CVC tephra deposits and the alkaline cinder cones. Data for the alkaline cinder cones are from Cai (2009). Isotopic data for the Group I and Group II samples were analyzed on Triton series TIMS instrument at Univ. Leeds as part of this study and analytical details can be found in Crummy (2013). Error bars are smaller than all the symbols used. Also shown are isotopic compositions for Nevado de Colima and Volcán Cántaro rocks after Verma and Luhr (2010). The Group I and the majority of the Group II eruption deposits show little variation in $^{87}Sr/^{86}Sr$ and $^{143}Nd/^{144}Nd$ with SiO_2 suggesting fractional crystallization from a relatively homogenous source. Two samples from unit F display isotopic compositions similar to those of the alkaline cinder cones, suggesting a common source, or mixing event

The cinder cone magmas have high $^{87}Sr/^{86}Sr$ (0.70381 to 0.70417) and low $^{143}Nd/^{144}Nd$ (0.51277 to 0.51287; Cai 2009) relative to the Group I eruption deposits and the majority of the Group II units (Fig. 10). Two samples from unit F of the Group II eruption deposits have similar isotopic compositions to two of the alkaline magmas consistent with mixing between isotopically distinct magmas.

The variation of $^{87}Sr/^{86}Sr$ versus $^{143}Nd/^{144}Nd$ for the calc-alkaline Group I and II eruption deposits, and the alkaline cinder cones reveals that all the CVC magmas fall within the mantle array (Fig. 11; Zindler and Hart 1986). Collectively, the CVC magmas appear to define a trend away from the estimated mantle wedge composition (Nimz et al. 1995; Gómez-Tuena et al. 2007) towards a more enriched component, with the alkaline cinder cone magmas having more enriched radiogenic isotopic signatures. Our findings, based on the new Sr and Nd isotope dataset, are in agreement with the Pb isotope ratios characteristic for CVC magmas reported by Verma and Luhr (2010).

5 Magmatic Evolution of the CVC

The geochemical and petrological variations shown by the CVC magmas reveal a heterogeneous source region in the mantle wedge under

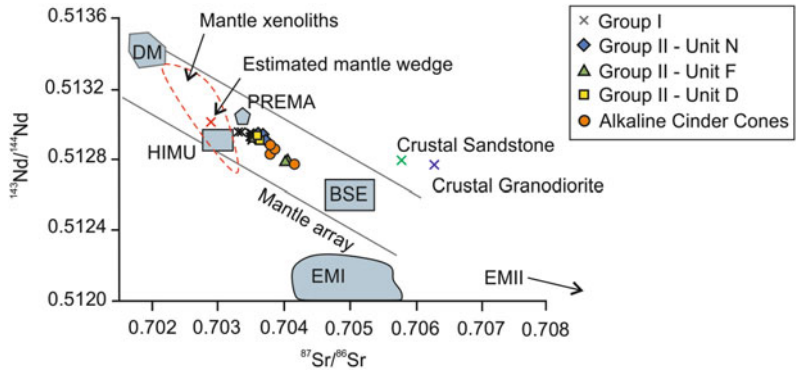

Fig. 11 $^{87}Sr/^{86}Sr$ versus $^{143}Nd/^{144}Nd$ diagram showing the relation of the CVC tephra deposits and the alkaline cinder cone magmas to the mantle reservoirs as defined by Zindler and Hart (1986). Data sources and analytical techniques and errors are the same as those on Fig. 10. Also shown are the mantle xenolith compositions from Northern Mexico (defined by dashed line; after Nimz et al. 1995), the estimated Mexican mantle wedge composition of Gómez-Tuena et al. (2007), and the compositions of granodiorite (Verma and Luhr 2010) and sandstone (Centeno-García et al. 1993) crustal rocks from the western Trans Mexican Volcanic Belt. The CVC magmas lie along the mantle array, trending towards a more enriched mantle source. The Group I and Group II eruption deposits appear to trend away from the mantle wedge composition towards the composition of the alkaline cinder cone samples

the CVC. The trace element abundance patterns displayed by CVC magmas are controlled by the influence of fluids from the subducting slab and the resulting partial melting of the overlying mantle. The fluid fluxing of the mantle wedge is responsible for fluid mobile element and LILE enrichments, while the relatively low HFSE abundances are controlled by residual mineral phases in the subducting slab (Tatsumi et al. 1992).

Incompatible trace element variation diagrams for the Group I and Group II calc-alkaline eruption deposits and the alkaline cinder cone magmas are shown in Fig. 12. Overall, the Group I eruption deposits form a cluster with no strong slab-derived fluid or sediment melt component (high Ba/Th, Ba/La, Ce/Pb and Th; Saunders et al. 1991; Schmidt and Poli 2004), and no strong slab-melt, or residual garnet signature (low La/Yb and Sr/Y coupled with Dy/Yb; Defant and Drummond 1990). The Group II eruption deposits display much stronger enrichments in Th suggesting a higher sediment component relative to the Group I samples (Fig. 12; Plank and Langmuir 1998). The opposite is displayed by the Ce/Pb ratio, with the Group II deposits containing higher concentrations of both Ce (70–130 ppm) and Pb (9–24 ppm) relative to the Group I samples (20–30 ppm Ce and 5–8 ppm Pb), indicating enrichment by both sediment melts and fluids. These deposits also show increasing Dy/Yb correlating with increasing La/Yb and Sr/Y reflecting contribution from a garnet-bearing source. The alkaline cinder cone magmas follow a similar trend to the Group II units, with a wide range of compositions reflecting fluid and sediment melt enrichment, and residual garnet in the source.

Several models have been proposed suggesting that the lamprophyric CVC magmas result from low degree melting of an enriched (veined) mantle source (Wallace and Carmichael 1989; Luhr 1997; Maria and Luhr 2008; Vigouroux et al. 2008). Such enriched metasomatic veins of phlogopite, clinopyroxene and apatite form as a result of the interaction of fluids from the subducting slab with depleted mantle wedge peridotites (Foley 1992). These veins have a lower melting point than the surrounding dry peridotite wall-rock, therefore low percentage melting is capable of producing the highly incompatible element-enrichments characteristic for the CVC lamprophyric melts (Foley 1992).

The elemental and isotopic data presented here supports models for alkaline mafic melt